



HAL
open science

New multi-rod linear actuator for direct-drive, wide mechanical band pass applications

Pierre-Emmanuel Cavarec, Hamid Ben Ahmed, Bernard Multon

► **To cite this version:**

Pierre-Emmanuel Cavarec, Hamid Ben Ahmed, Bernard Multon. New multi-rod linear actuator for direct-drive, wide mechanical band pass applications. IEEE IAS annual Meeting 2002, Oct 2002, PITTSBURG, United States. 8pp. hal-00674668

HAL Id: hal-00674668

<https://hal.science/hal-00674668>

Submitted on 27 Feb 2012

HAL is a multi-disciplinary open access archive for the deposit and dissemination of scientific research documents, whether they are published or not. The documents may come from teaching and research institutions in France or abroad, or from public or private research centers.

L'archive ouverte pluridisciplinaire **HAL**, est destinée au dépôt et à la diffusion de documents scientifiques de niveau recherche, publiés ou non, émanant des établissements d'enseignement et de recherche français ou étrangers, des laboratoires publics ou privés.

New multi-rod linear actuator for direct-drive, wide mechanical band pass applications

P.E. Cavarec, H. Ben Ahmed, B. Multon

LESiR-SATIE (UMR CNRS 8029)

ENS de Cachan - Brittany Branch Ker Lann Campus, 35170 Bruz FRANCE

e-mail: cavarec@bretagne.ens-cachan.fr

Abstract: *In this article, a new multi-rod linear actuator is presented. This actuator has been developed for high thrust density and wide mechanical band pass applications. The multi-airgap concept will first be illustrated and explained. Its advantages will be highlighted thanks to finite element method optimizations. Next, the multi-rod prototype technology will be discussed. Lastly, experimental measurements for prototype forces will be provided.*

I. Introduction

In electrical drives, load is generally linked to the actuator by means of mechanical transmission (e.g. gears). This mechanical transmission is required in order to adapt the load to a standard motor (as regards type of movement, speed).

In a growing number of instances, direct drives are preferred to mechanical transmission for several reasons [1]. Direct drives enable:

- replacing gears (hence saving cost),
- reducing noise,
- increasing movement control,
- widening the mechanical band pass,
- lowering maintenance.

For automation applications, such as command (plane command, hard disk harm) or regulation (vibration compensation), mechanical band pass represents the primary constraint. For both of these (command and regulation), the system's mechanical time constant proves to be greatest (the sensor, computing and command time constants are all generally lower). Direct drives (i.e. featuring no mechanical transmission) present two main advantages in such applications:

- They eliminate the mechanical tolerance that causes the "backlash" phenomenon and thus lowers precision. Moreover, they introduce a sleep time into the feedback loop.
- From an overall perspective, the reduction level serves to increase system inertia due not only to inertia of the mechanical transmission itself, but to the actuator inertia as well.

The main difficulty for direct drives consists of reaching sufficient force density (i.e. force for a linear actuator, torque for a rotary actuator). The absence of gears imposes a considerably higher force. For electromagnetic actuators however, the size (and thus cost) is linked to this force (we recall herein that for electronic power converters, cost is linked to apparent power). For low-speed movement, direct drives are therefore of interest once a sufficiently high force-to-volume ratio has been reached.

II. Multi-airgap linear actuators

In electromagnetic actuators, the mechanical constraints of a magnetic airgap cannot be overcome: the magnetic shear stress gets limited by means of both airgap induction and electrical loading. In turn, airgap induction is limited by the saturation of ferromagnetic materials and electric loading is limited by heating and/or demagnetization of any eventual magnets. With a copper conductor, the maximum attainable values of airgap shear stress rarely exceed 10 to 20 N/cm². An actuator can thereby be described as a system for producing magnetic fields that interact inside an airgap where magnetic stress is being generated.

Another approach [2], conceived some twenty years ago yet still rather undeveloped due to its conceptual complexity, consists of splitting the active zone so as to increase airgap surfaces, thus giving rise to what are called "multi-airgap structures".

A. The various types of global-coil, multi-airgap actuators

Splitting the active zone may be performed in two ways: the coil may be split (in split-coil actuators) or kept whole (in global-coil actuators).

Split-coil actuators may be viewed as the summation of several single-airgap actuators. This category primarily features multi-discoid actuators.

For the global-coil actuator, either a variable reluctance (VR) actuator or permanent magnet actuator is possible. VR actuators exhibit two kinds of patterns: a longitudinal flux pattern and a transverse flux pattern, as depicted below:

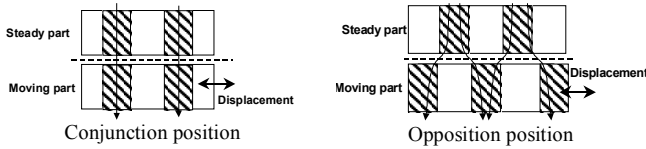


Fig. 1a: Transverse flux reluctance pattern

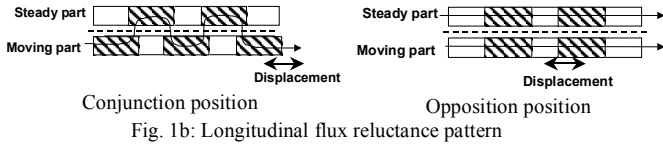


Fig. 1b: Longitudinal flux reluctance pattern

For permanent magnet actuators, four kinds of patterns exist: longitudinal flux and magnet (A-pattern), longitudinal flux and transverse magnet (B-pattern), transverse flux and longitudinal magnet (C-pattern), and transverse flux and magnet (D-pattern), as follows:

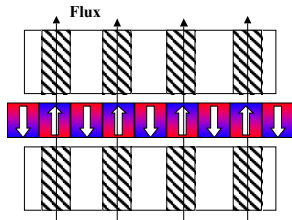


Fig. 2a: A-pattern, positive conjunction

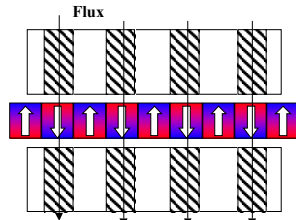


Fig. 2b: A-pattern, negative conjunction

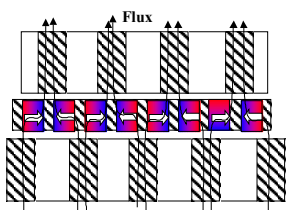


Fig. 3a: B-pattern, positive conjunction

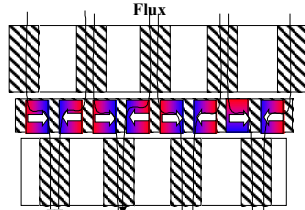


Fig. 3b: B-pattern, negative conjunction

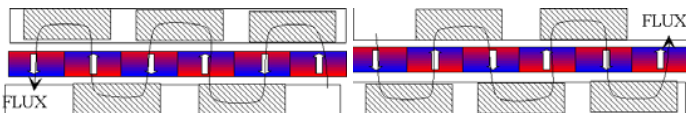


Fig. 4a: C-pattern, positive conjunction

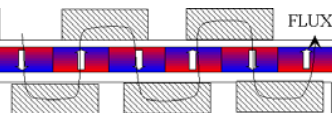


Fig. 4b: C-pattern, negative conjunction

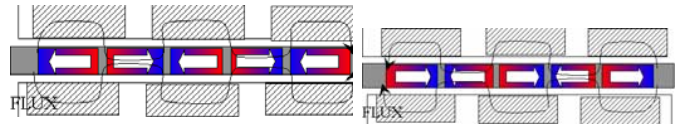


Fig. 5a: D-pattern, positive conjunction

Fig. 5b: D-pattern, negative conjunction

In general, the transverse flux pattern is well-adapted to rotary actuators and the longitudinal flux pattern to linear actuators.

B. Benefit of global-coil, multi-airgap actuators

In order to demonstrate the benefit of multi-airgap structures, we have compared [9] two basic permanent magnet actuator architectures (i.e. split-coil, multi-airgap and global-coil, multi-airgap) with the C-pattern [3], thereby yielding:

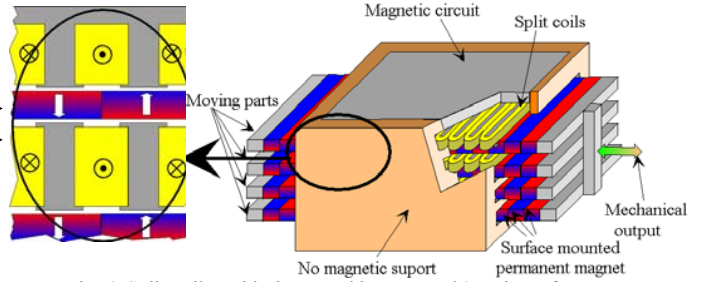


Fig. 6: Split-coil, multi-airgap architecture and 3D view of one phase of an actuator

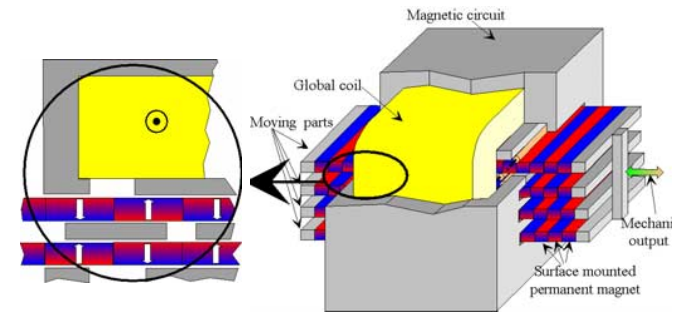


Fig. 7: Global-coil, multi-airgap architecture and 3D view of one phase of an actuator

These structures have been optimized thanks to a genetic algorithm tied to a finite element method (FEM). The force calculation, based on the flux/magnetomotive force, will be presented in Section III for the multi-rod prototype.

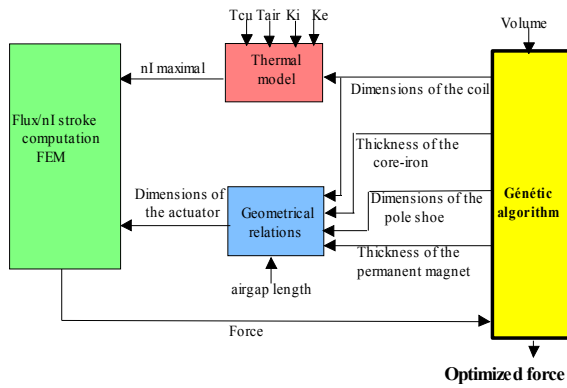


Fig. 8: Diagram of the optimization method

A comparison of the force-to-volume ratio for various volumes helps summarize these results. In the present case, both the airgap thickness (1 mm) and cooling conditions (airflow cooling on the exterior surface) are the same for the two types of actuators:

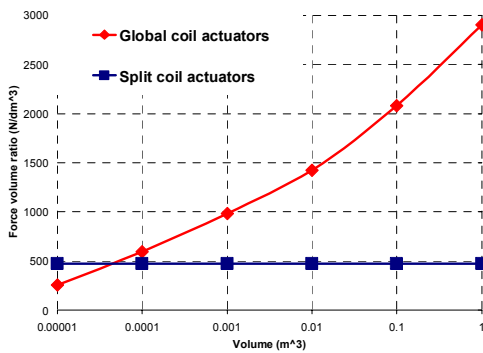


Fig. 9: Scale effect on force-to-volume ratio for optimized multi-airgap architectures of linear actuators

It can be concluded that under given cooling conditions, a volume always exists for which global-coil actuators outperform split-coil actuators. This volume is linked directly to airgap thickness: as the airgap narrows, the multi-airgap actuators become more effective.

III. The new multi-rod actuator

A. General presentation of the multi-rod actuator

The actuator presented herein is the result of our previous experimental work with multi-airgap actuators [3,4,5]. Its introduction has been focused on wide band pass applications. The mechanical set-up has been designed to minimize airgap thickness. In order to enhance mechanical precision, all of the mobile parts are rods.

This cylindrical shape leads to the D-pattern, which features an axis of symmetry. Permanent magnets are placed on the static part of the actuator. The mobile rods are composed of a succession of magnetic and non-magnetic rings.

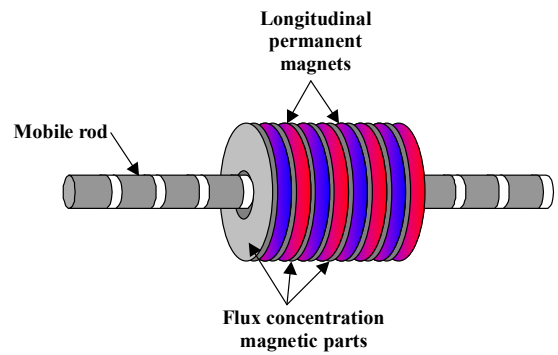


Fig. 10a: Elementary pattern in the multi-rod actuator

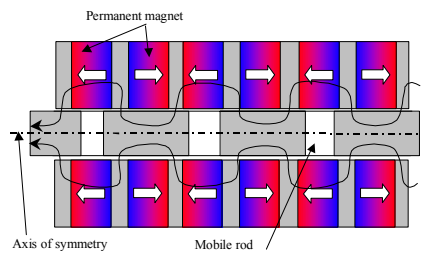


Fig. 10b: Positive conjunction

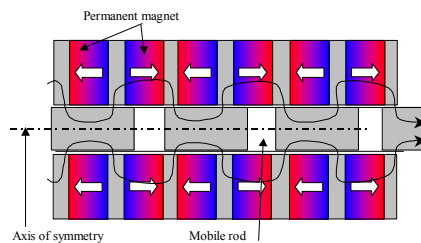


Fig. 10c: Negative conjunction

Three phases have been placed along the rods, as follows:

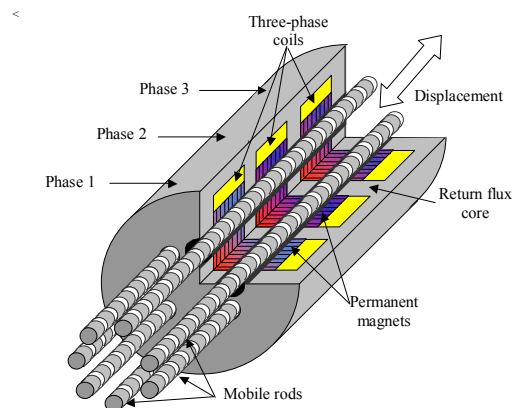


Fig. 11: Operating principle of the multi-rod actuator



Fig. 12: Multi-rod prototype

B. Finite element method computation

The significant mechanical complexity herein has prevented us from conducting a global simulation of the actuator. The same methodology as in Section 2 has thus been applied, with only an elementary pattern being modeled by the Finite Element Method.

First, the magnetic salience of the pattern was calculated. This result yielded an L_d/L_q ratio of 0.984. Hence, we may neglect the reluctance force in this pattern. Under these conditions, we decided to limit our study to just the conjunction positions. Intermediate flux positions were then extrapolated between these two conjunction positions.

Thanks to the axial symmetry of the pattern, a 2D Finite Element Method can be used. The following figure displays the field map of the FEM simulation.

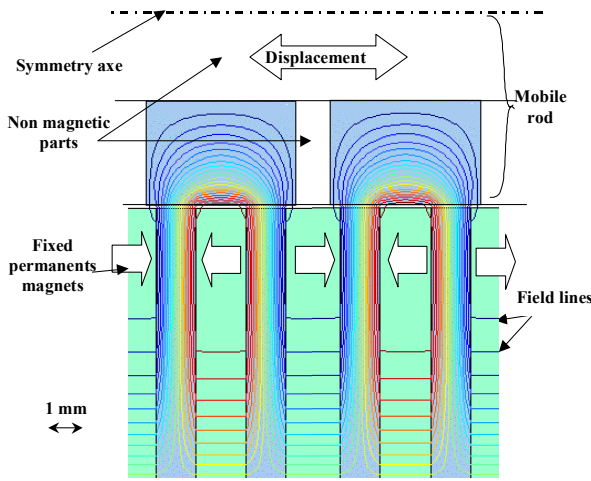


Fig. 13: Permanent magnet flux in the conjunction position of two elementary patterns

It should be noted that in employing such an approach, the flux return part of the actuator is considered to be perfect.

These calculations give the extreme curves of the flux of each pattern as a function of the magnetomotive force being applied on each of them.

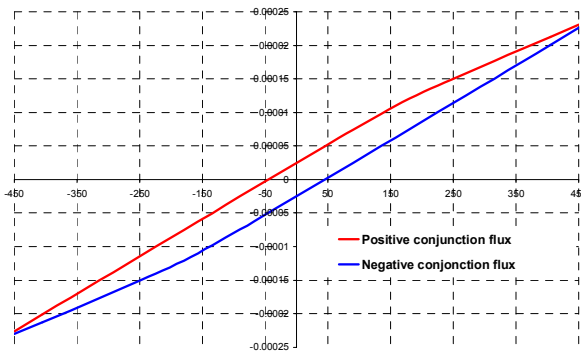


Fig. 14: Flux/M.M.F. extreme curves of the pattern

Using these results, the extreme flux-magnetomotive force of the total actuator has been calculated. The actuator has 8 rods in parallel, with each of the three phases being composed of 8 elementary patterns in series. The flux and

M.M.F. of an elementary pattern are hence multiplied by 8 in the actuator.

Two types of supplies have been considered herein: square-wave current and sinusoidal current.

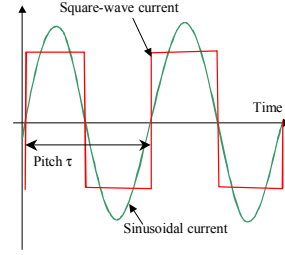


Fig. 15: Square-wave current and sinusoidal current for the same RMS value

The square-wave current actuator force is simple to calculate by applying the conversion energy theory: for each stroke (pitch τ) of the multi-rod motor, an energy W_m is converted from an electrical form to an electromagnetic form. With square-wave currents, this energy can be expressed as:

$$W_m = \oint_{ni} \phi(nI).dnI = 2 \cdot \int_{-nI_{\min}}^{nI_{\max}} \phi(nI).dnI \quad (1)$$

The average electromagnetic force \bar{f} then equals:

$$\bar{f} = \frac{W_m}{\tau} \quad (2)$$

The converted energy W_m can be graphically calculated on the flux/magnetomotive loop. For square-wave currents, the following figure shows two loops for RMS current values of 15.75 A (2520 At) and 6.75 A (1080 At):

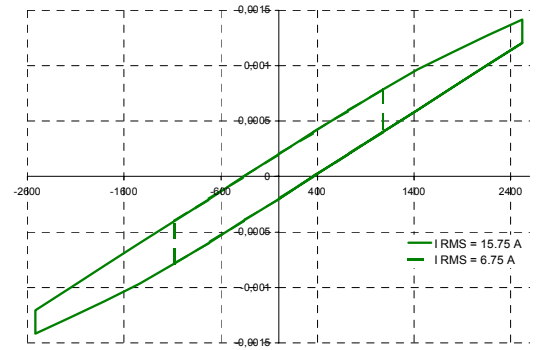


Fig. 16: Flux/magnetomotive actuator loop with square-wave current

For the sinusoidal current, Equation (2) remains valid. Moreover, the converted energy W_m is still represented on the flux/magnetomotive force loop. This loop has been drawn in considering that for a given current, flux variation is sinusoidal. The following figure presents the loop for RMS currents of 15.9 A and 8 A, respectively.

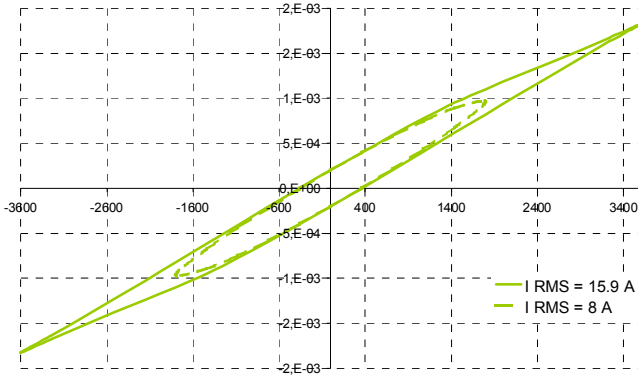


Fig. 17: Flux/magnetomotive actuator loop with sinusoidal current

By virtue of Equation (2), we can then proceed with calculating the force as a function of RMS current for two kinds of current:

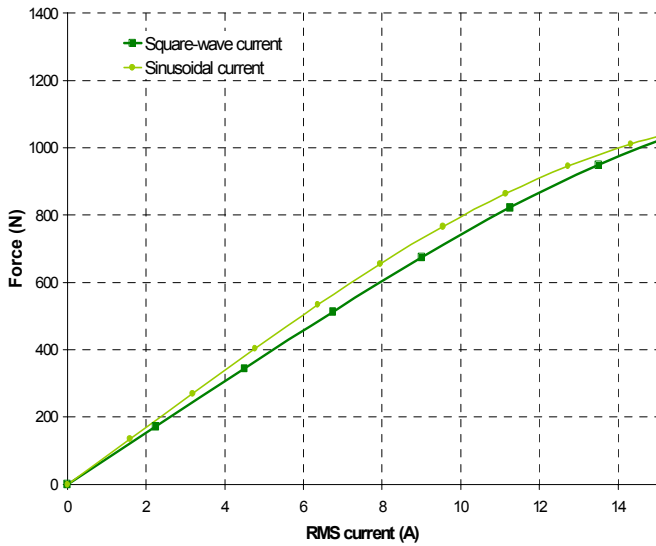


Fig. 18: Force vs. RMS current

For the linear part of the curve, the ratio between the square wave-fed actuator force and the sinusoidal force is:

$$\frac{F_{\sin}}{F_{\text{square}}} = \frac{\pi}{2\sqrt{2}} \approx 1.11 \quad (3)$$

In contrast, saturation of magnetic parts limits the maximum conversion energy to a common value for both types of supply: the two curves do not intersect.

C. Normal forces and mechanical guidance of the multi-rod actuator

One of the most difficult aspects in multi-airgap actuators pertains to the mechanical guidance. In order to obtain a very high force-to-volume ratio, airgap thickness must be minimized. Given that the maximum speed of the actuator is relatively low (less than $2.5 \text{ m}\cdot\text{s}^{-1}$), contact guidance is possible, yet the normal forces prove unstable. The solution of spread guidance has been adopted so as to minimize eccentricity and thereby the resulting normal forces.

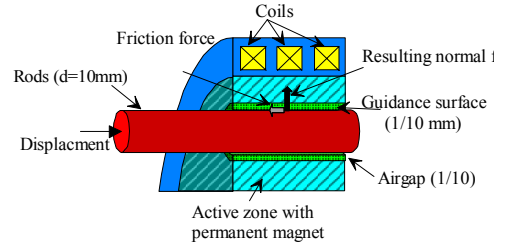


Fig. 19: Spread guidance operating principle

In order to avoid hyperstaticity, each mobile rod is mechanically independent. Guidance surfaces, composed of Teflon® sheets, have been placed around each of the rods.

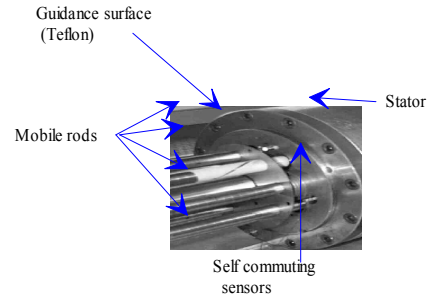


Fig. 20: Spread guidance set-up

IV. Static forces and dynamic behavior in the multi-rod actuator

A. Static force of the multi-rod actuator

Static force has been measured using the uncoupled method: coils are fed by direct current and a force sensor gives the maximum mechanical resistance of the actuator. Hence, we are able to measure the static electromagnetic force plus the friction force.

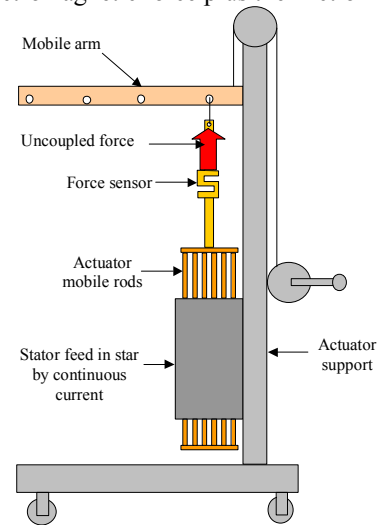


Fig. 21: Uncoupled test principle

The pertinent results can be summed up in the following figure:

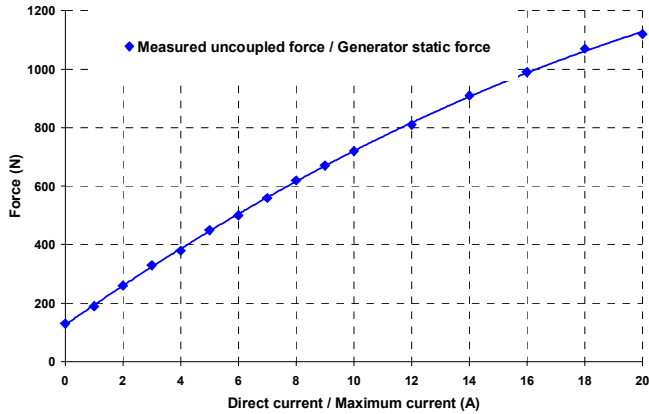


Fig. 22: Static force vs. maximum current

The friction force is estimated at 130 N.

Since the cogging force due to the permanent magnet is very low (less than 10 N), this uncoupled test produces the force of the self-commuted actuator under generator conditions as a function of maximum current.

In order to derive the force as a function of RMS current, the current scale would have to be modified.

The motor force is equal to the generator force minus twice the friction force.

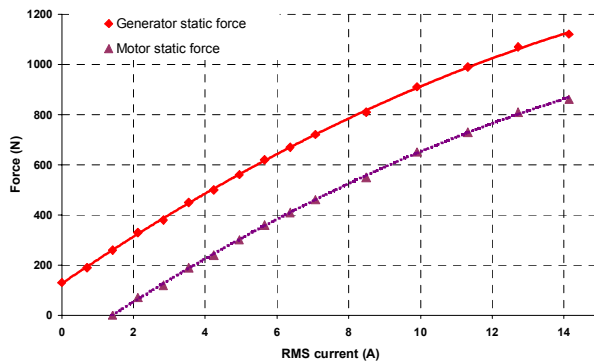


Fig. 23: Generator and motor static forces vs. current

Given that the magnetic salience is very low, the optimal self-commutation angle between the current and the EMF is close to 0° (which means that no reluctance force is present).

We will now compare the low-speed electromagnetic force (without friction and magnetic losses) to the simulation results under sinusoidal current conditions. Moreover, the EMF has already been measured; it can yield the slope of the force over the linear part of the curve.

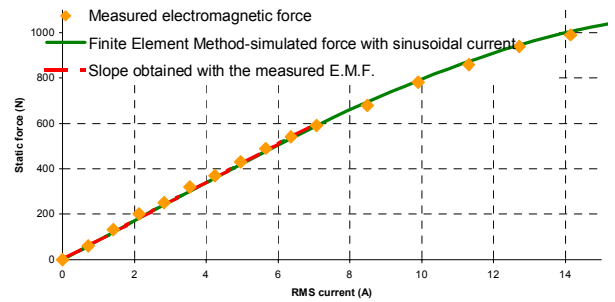


Fig. 24: Low-speed force comparison between static measurements and FEM simulation

We are able to state that the measurements show a very close fit with simulation values.

The overall volume of this actuator is about 1 dm^3 . Measurements indicate a maximum electromagnetic force of 1000 N. We have therefore reached a force-to-volume ratio of 1000 N/dm^3 , which is three times the value obtained for classical electromagnetic linear actuators ($\approx 300 \text{ N/dm}^3$).

We can conclude that this multi-rod actuator serves to validate the theoretical interest of multi-airgap actuators for high force-to-volume ratios.

B. Self-commutation

In order to self-commute the actuator, integrated sensors have been developed that make use of the actuator rod [7]; these sensors are designed to be automatically synchronous with the actuator position.

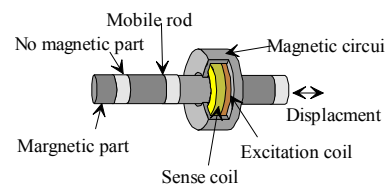


Fig. 25: Electromagnetic structure of the sensor

They have been optimized for maximum compaction (see Fig. 20).

One of the difficulties in self-commutation within such an actuator concerns the load. The mechanical time constant is very low and depends on the friction force. An adapted linear load is required to carry out self-commutation.

We have chosen a passive inertial load, as shown in Figure 26. This mass is composed of 5-kg modular elements and has been placed on a linear motion guide. A car damper can be added, for example, to increase the load losses.

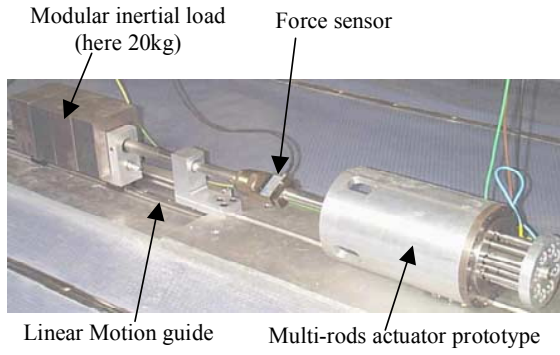


Fig. 26: Mechanical load of the multi-rod actuator prototype

Self-commutation with a three-phase converter is currently being tested on this pure inertial load.

C. The scaling effects for wide mechanical band pass applications

Wide mechanical band pass linear applications have been introduced in numerous instances. The following can be cited for purposes of illustration:

- compensation of high-speed train vibrations,
- parallel robots for the high-speed manipulation of heavy loads,
- plane aileron commands.

This wide mechanical band pass may be expressed relatively well by the maximum acceleration of the linear load. For the sake of simplicity, we will consider the load as a pure inertial load.

For linear movement, we can compare two kinds of solutions:

- the classical "screwball" system, in which a ball screw is placed between the rotative electrical actuator and the linear load; and

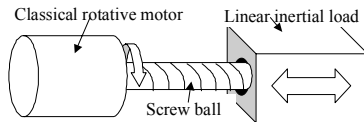


Fig. 27: Indirect linear actuator: "screwball" system principle

- the direct-drive solution, in which the linear electrical actuator is directly linked to the linear load.

For the "screwball" solution, a key parameter is the coefficient of conversion k between the linear movement and the rotative movement ($k = \frac{\Omega}{v}$). With a rotative

actuator, the internal inertia is called J and the nominal torque T_n . If the linear load were a pure inertial load of mass M , the linear acceleration would be:

$$a = \frac{T_n \cdot k}{M + k^2 \cdot J} \quad (4)$$

The optimal value (acceleration maximization) of k is:

$$k_{opt} = \sqrt{\frac{M}{J}} \quad (5)$$

With this value, the maximum acceleration becomes:

$$a_{max} = \frac{T_n}{2 \cdot \sqrt{J}} \cdot \frac{1}{\sqrt{M}} \quad (6)$$

The first part of this equation relates to the actuator: this value is directly linked to the size of the actuator. The scaling effect gives the evolution of torque and inertial load as a function of dimension l^* [8].

For a thermal operating point, the nominal torque of the rotating permanent magnet motor is:

$$\frac{T_n}{V} \propto l^{*0.5} \cdot k_e^{0.5} \quad (7)$$

where k_e is the thermal coefficient (expressed in terms of $W \cdot m^{-2} \cdot K^{-1}$).

The rotor inertia is:

$$J \propto l^{*5} \quad (8)$$

Hence, maximum acceleration is linked to the size of the actuator as follows:

$$a_{opt} \propto \frac{l^{*3.5} \cdot k_e^{0.5}}{2 \cdot l^{*2.5}} \cdot \frac{1}{\sqrt{M}} \propto \frac{l^*}{\sqrt{M}} \quad (9)$$

For a direct-drive linear actuator, two kinds of actuator can be chosen:

- classical linear permanent magnet synchronous motors
- multi-rod actuators.

For both solutions, the mobile part of the actuator is very lightweight. For our prototype, the rods weigh around 1.3 kg and are thus negligible in comparison with the weight of the load. The acceleration is:

$$a = \frac{F_n}{M} \quad (10)$$

where the nominal force is linked to the size of the actuator.

Classical linear permanent magnet synchronous motors display, under given thermal conditions, a constant force-to-volume ratio [9]:

$$\frac{F_n}{V} \propto k_e^{0.5} \quad (11)$$

The maximum acceleration follows the scaling rule:

$$a \propto \frac{l^{*3}}{M} \quad (12)$$

The same scaling effect can then be applied to the multi-rod actuator [9]:

$$\frac{F_n}{V} \propto \frac{l^{*0.5} \cdot k_e^{0.5}}{e} \quad (13)$$

where e is the airgap, linked to a mechanical technology. For our purposes, we will maintain a constant airgap. The maximum acceleration follows the scaling rule:

$$a \propto \frac{l^{*3.5}}{M} \quad (14)$$

For our multi-rod actuator, for instance, $l^* = 0.1$ m ($V = 1$ dm³):

$$F_n = 1000 \text{ N}$$

For the same volume (1 dm³), the force of a classical permanent magnet synchronous motors is approximately:

$$F_n = 300 \text{ N}$$

Without taking the inertia and ball screw volume into account, the best rotative actuator has the following values:

$$T_n = 3.3 \text{ Nm}$$

$$J = 0.17 \cdot 10^{-3} \text{ kg.m}^2$$

The scaling effect provides two system comparisons: light load ($M=10$ kg - $k=242$ rad/m), and heavy load ($M=100$ kg - $k=767$ rad/m).

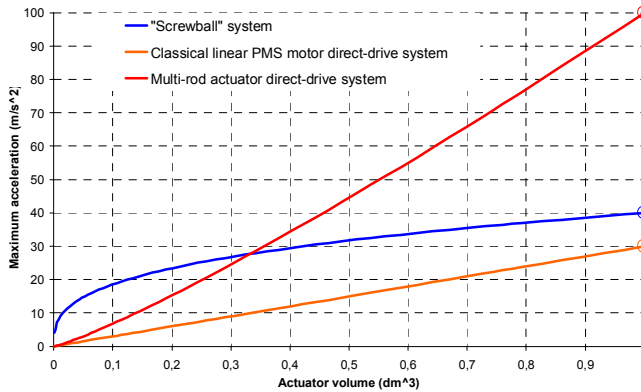


Fig. 28a: Maximum acceleration for a linear inertial load of 10 kg vs. actuator volume

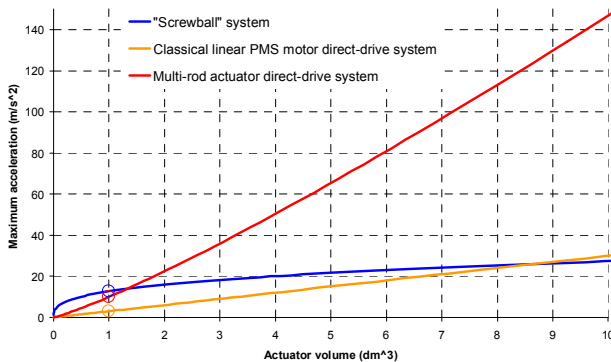


Fig. 28b: Maximum acceleration for a linear inertial load of 100 kg vs. actuator volume

On Figures 28a and b, the reference values have been represented by an empty circle. It is apparent that direct-drive systems become worthwhile only once acceleration has reached high levels. This efficiency increases with heavier loads.

V. Conclusion

This paper has focused on a new multi-airgap synchronous actuator dedicated to high mechanical band pass applications.

The Finite Element Method has yielded results very comparable to measurements with the multi-rod prototype under sinusoidal current conditions, despite a very complex magnetic structure.

The performances of this actuator are very attractive (around 1000 N/dm³ with a force of 1000 N) and prove the interest of the multi-airgap technology.

Mechanical guidance problems have been resolved thanks to an original spread guidance solution. We are now working towards minimizing the normal force and searching the best compromise between tangential and normal forces.

Furthermore, the theoretical advantages of direct-drive solutions for wide mechanical band pass applications have been demonstrated.

VI. References

- [1] B. Multon and J. Bonal, "Electromechanical direct drives: Variety, constraints and solutions", *Electrical Engineering Review (REE in French)*.
- [2] C. Rioux, « Théorie générale comparative des machines électriques établie à partir des équations du champ électromagnétique », *R.G.E.*, May 1970, Tome 79, n° 5, pp. 415-421.
- [3] P.E. Cavarec *et al.*, "Advantage of Increasing the Number of Airgap Surfaces in Synchronous Linear Actuators", *Electromotion 2001*, Bologna, Italy, pp. 251-256, June 19-20, 2001.
- [4] H. Ben Ahmed, L. Prévond, B. Multon, B. Salamand and J. Lucidarme, "Special Synchronous Linear Actuators: Structures and Performances", *Revue Electromotion*, n°5, 1998, pp. 93-101.
- [5] P.F. Desesquelles, J. Lucidarme and H. Ben Ahmed, "Theoretical and Experimental Results On Multi-Airgap Axial Synchronous Machines With Permanent Magnets", *ICEM '90*, Cambridge, Mass. (USA), August 1990.
- [6] Matt, R. Goyet, J. Lucidarme and C. Rioux, "Longitudinal Field Multi-Airgap Linear Reluctance Actuator", *Electric Machines & Power Systems*, 1987, 13:299-313.
- [7] P.E. Cavarec *et al.*, "Integrated reluctance position sensor for the self-commutation of a hybrid linear electric actuator", *CD-ROM Proceedings, E.P.E.*, August 2001, Graz.
- [8] M. Jufer *et al.*, "Laws governing the size reduction of electromechanical transducers with applications to step motors", Department of Electrical Engineering, University of Illinois, Urbana-Champaign, 1974.
- [9] P.E. Cavarec *et al.*, "Force Density Improvements from Increasing the Number of Airgap Surfaces in Synchronous Linear Actuators", *IEE Proceedings, Electric power application* (accepted with revisions, May 2002).